Fuel Cells Bulletin
ISSN: 1464-2859

Impact of Promoting Fuel Cell Vehicles on Urban Air Quality and Health Benefits

Wanyuan Yang*, Cheng Li

School of Automobile, Chang'an University, Xi'an 710086, Shaanxi, PR China

Corresponding Author: Wanyuan Yang, Email: 2022122057@chd.edu.cn

Abstract: Fuel cell vehicles (FCVs) are considered a promising clean energy transportation option with significant potential to alleviate urban air pollution. However, their environmental benefits are not fixed but are influenced by various factors, including vehicle usage patterns and road conditions, which in turn affect air quality and public health. This study takes Xi'an as a case study and employs the COPERT model to develop a 2020 emission inventory for FCVs. Future vehicle ownership in 2035 is projected under low, medium, and high electrification scenarios using multiple models. The WRF-SMOKE-CMAQ modeling system is utilized to simulate air quality changes, while the BenMap-CE model is applied to assess health benefits. The results indicate that under the high electrification scenario, pollutant emissions are reduced by 64.59%–88.86% compared to 2020 levels, with pollutant concentrations exhibiting a gradient distribution along the road network. In winter, CO, NO_2, and $PM_{2.5}$ concentrations are significantly higher than in summer. Improved air quality leads to substantial health benefits related to $PM_{2.5}$, with the high electrification scenario preventing an estimated 770 premature deaths and generating up to 400 million CNY in economic benefits. These findings demonstrate that the widespread adoption of FCVs can effectively reduce urban traffic-related pollution burdens and yield significant environmental and health co-benefits, providing a scientific basis for clean transportation policymaking.

Keywords: Fuel Cell Vehicles; Air Quality; Pollutant Emissions; Health Benefits; Clean Transportation P olicy

1. Introduction

With the rapid development of the economy and society and the acceleration of urbanization, people's quality of life and modes of transportation are also undergoing significant changes, leading to an explosive growth in motor vehicle ownership[1]. Due to the uneven economic development and population growth, the current imbalance in motor vehicle ownership poses a severe challenge to improving regional environmental quality and public health. Measures need to be taken to reduce traffic emissions and improve traffic management to mitigate the adverse effects on the environment and health. In recent years, China has implemented multiple measures to improve air quality. The promotion of new energy vehicles and the replacement of old, high-emission vehicles have effectively reduced vehicle exhaust emissions. At the same time, the vigorous development of clean energy has reduced reliance on traditional coal, thereby lessening the adverse impact of coal-fired power generation and heating on air quality.

Fuel cell vehicles (FCVs) have lower emissions and do not directly emit pollutants such as NOx, PM, and VOC, which are the main contributors to air pollution and health hazards. However, the existence of fuel-powered vehicles poses a challenge to this goal. The road transport sector consumes a large amount of fossil fuels, such as oil and natural gas, and fuel-powered vehicles are the direct users of these resources, causing significant environmental harm and being major contributors to atmospheric pollutant emissions[2]. The development of FCVs is considered an effective means to address the atmospheric pollution caused by vehicle emissions and improve human exposure to pollutants. FCVs can even achieve "zero emissions" in the road transport sector. The increasing popularity of FCVs has prompted many cities around the world to explore their potential for improving air quality. Meanwhile, more and more countries are enacting regulations to limit the sale of fuel-powered vehicles and promote the development of the electric vehicle industry. Countries such as Norway, the Netherlands, the United Kingdom, and Germany have announced plans to gradually ban the sale of fuel-powered vehicles in the future[3]. The development of electric vehicles is conducive to improving energy efficiency and air quality.

As the world moves towards more sustainable modes of transportation, such as the promotion and popularization of FCVs, it is necessary to conduct in-depth research on the actual impact of FCVs on urban air quality and human health. This research is crucial as it can provide critical insights to guide policymakers and social decision-makers in taking more effective measures to improve the urban environment and promote public health. The Chinese government has proposed multiple policies and initiatives to promote the development of the electric vehicle industry, in response to the national commitment to reducing air pollution and improving public health. Urban air quality has been a major concern in many Chinese cities, with high concentrations of particulate matter and other pollutants affecting the health of millions of people. FCVs are seen as a promising solution to pollution problems, as they emit far lower levels of pollutants compared to traditional fuel-powered vehicles[4][5][6].

Existing studies have shown that the promotion of FCVs can significantly reduce pollutant emissions, but their actual environmental benefits are constrained by factors such as the source of hydrogen production, vehicle usage patterns, and geographical and meteorological conditions[7][8][9]. For example, if hydrogen production relies on fossil fuels, the indirect emissions of FCVs may undermine their emission reduction potential. Additionally, the health effects of changes in pollutant concentrations need to be economically quantified in combination with exposed populations and disease burdens to provide scientific support for policy-making. Therefore, this study focuses on Xi'an City, constructing an emission inventory under multiple hydrogen energy scenarios, coupling an air quality model (WRF-SMOKE-CMAQ) and a health benefit assessment tool (BenMap-CE), to quantify the impact of different hydrogen energy pathways on the concentrations of pollutants such as $PM_{2.5}$ and NO_2, and to assess the avoidable premature deaths and economic losses, providing a basis for the green transformation of urban transportation.

2. Materials and Methods

2.1 Study Area

Xi'an, the largest central city in Northwest China and a typical Chinese megacity, serves as one of the major nodal cities in the national trunk highway network. Geographically, Xi'an is situated between 107°40′–109°49′ east longitude and 33°42′–34°45′ north latitude, within the Guanzhong Basin in the middle reaches of the Yellow River (Fig.1). Additionally, Xi'an is one of the demonstration cities for new energy vehicles (NEVs). With the rapid development of the new energy industry in recent years, the number of NEVs in Xi'an has continued to rise. In 2022, Xi'an's NEV production exceeded 1 million units, representing a year-on-year increase of 277.5%, accounting for 14.1% of China's total production and ranking first in the country that year. However, according to a 2021 report by the Ministry of Ecology and Environment, Xi'an's air quality remains suboptimal, ranking low among 168 cities in China, with polluted days accounting for 27.4% of the year. Motor vehicles are a significant source of air pollution in large and medium-sized cities, and Xi'an, with its large and rapidly growing vehicle fleet, had 4.091 million vehicles in 2021, a 9.54% increase from 2020. Therefore, reducing traffic emissions is a critical task for improving air quality.

Fig.1. Geographic Location of the Study Area

2.2 Scenario Description

Xi'an City plans to vigorously develop new energy vehicles in the coming years to promote environmental protection and sustainable development. Specifically, for newly registered vehicles purchased by individuals, the target is to achieve a proportion of new energy vehicles of around 50% by 2025. Additionally, Xi'an will accelerate the electrification process in the public sector, striving for comprehensive electrification. For heavy-duty trucks and engineering vehicles, the penetration rate of new energy vehicles will be increased, with the goal of achieving full electrification by 2030. By 2035, battery electric vehicles will become the mainstream of newly sold vehicles, and public sector vehicles will be fully electrified. Based on the aforementioned policy documents, this study constructs low, medium, and high electrification scenarios for 2035, with the settings for different electrification scenarios detailed in Table 1 and Table 2.

Table 1. FCVs electrification rates (%) for different vehicle types in Xi'an under low, medium, and high scenarios in 2035.

Electrification Scenario	Buses and Taxis	LDV	MDV	HDV	LDT	MDT	HDT
Low Electrification	100	50	50	20	30	10	5
Medium Electrification	100	70	70	30	50	20	10
High Electrification	100	100	100	40	70	30	15

Table 2. BEVs and HEVs electrification rates (%) for different vehicle types in Xi'an under low, medium, and high scenarios in 2035.

Electrification Scenario	Buses and Taxis	LDV	MDV	HDV	LDT	MDT	HDT
Low Electrification	-	50	50	80	70	90	95
Medium Electrification	-	30	30	70	50	80	90
High Electrification	-	-	-	60	30	70	85

In this study, the electrification rate refers to the proportion of vehicles using electricity as the sole power source, and electrification scenarios refer to vehicle power source scenarios under different electrification rates. New energy vehicles include battery electric vehicles, hybrid electric vehicles, and fuel cell vehicles. Battery electric vehicles are those entirely powered by electricity stored in batteries; hybrid electric vehicles are those using both batteries and other fuels as power sources; and fuel cell vehicles are those powered by electricity generated from onboard fuel cells.

2.3 Emission Calculation

The vehicle population (VP), annual vehicle kilometers traveled (VKT), and emission factor (EF) are the primary factors influencing vehicle emissions. To establish an emission inventory for vehicles in Xi'an, the annual emissions of CO2 and pollutants from fuel-powered vehicles in the Xi'an region are estimated using the formula (1):

$$E_{n,i} = \sum_{j}\sum_{f}\sum_{k} VP_{j,f,k,i} \times VKT_{j,i} \times EF_{j,f,k,n} \times 10^{-6} \quad (1)$$

In the formula, E represents the annual emissions (tons); VP, VKT, and EF denote the vehicle population, annual average mileage, and emission factor, respectively; i represents the year, including 2021, 2022, 2023, ..., 2035; j refers to the vehicle type, with vehicles categorized in this study as light-duty trucks (LDT), medium-duty trucks (MDT), heavy-duty trucks (HDT), light-duty passenger vehicles (LDV), medium-duty passenger vehicles (MDV), heavy-duty passenger vehicles (HDV), taxis (TAXI), and buses (BUS); f indicates the fuel type, including gasoline, diesel, methanol, compressed natural gas (CNG), etc.; k represents the emission standard compliance of the vehicle, ranging from National I to National VI; n denotes the type of emissions, including pollutants (BC, CO, SO2, NOX, PM2.5, VOC, NH3), where PM2.5 emissions sources include wear emissions (tire wear, brake wear, and road wear) and vehicle exhaust emissions.

2.4 Car Ownership Forecast

As automobiles, particularly light-duty passenger vehicles, are typical durable goods, their population dynamics align with the Gompertz curve characteristics. Therefore, this study employs the Gompertz model to predict the population of light-duty passenger vehicles from 2021 to 2035[10][11]. The calculation formula is shown in (2):

$$V_i = V^* \times e^{\alpha e^{\beta x_i}} \quad (2)$$

In the formula, i represents the year (2011-2035); denotes the per thousand population ownership of light-duty passenger vehicles in year i (/1000); represents the ultimate saturation level of light-duty passenger vehicles in the region, expressed as per thousand population ownership, with the saturation level set at 0.45 based on the economic growth rate of Xi'an; represents the per capita GDP in year i; and are parameters reflecting the relationship between the changes in light-duty passenger vehicle ownership and economic level.

The elasticity coefficient method, which adopts a qualitative and quantitative approach to predict vehicle ownership based on the relationship between economic indicators and vehicle development, yields more accurate results and is suitable for macro-level forecasting[12]. Therefore, this study employs the elasticity coefficient method to predict the ownership of these vehicle types from 2021 to 2035, as shown in formulas (3) to (5):

$$VP_{i,j} = VP_{2020,i} \times \left(1 + \alpha_{i,j}\right)^{j-2020} \quad (i\in[2021,2035] \text{ and } i\in N) \quad (3)$$

$$\alpha_{i,j} = \varepsilon_j \times \beta_{i,j} \quad (i\in[2021,2035] \text{ and } i\in N) \quad (4)$$

$$\varepsilon_j = \frac{1}{10}\sum_{i=2010}^{2020} \frac{\alpha_{i,j}}{\beta_{i,j}} \quad (i\in[2010,2020] \text{ and } i\in N) \quad (5)$$

In the formula, i represents the year, j denotes the vehicle type, VP stands for vehicle population, represents the growth rate of vehicle population for type j in year i, represents the annual growth rate of per capita GDP in year i, and represents the elasticity coefficient for vehicle type j. The vehicle population data for light-duty trucks, medium-duty trucks, heavy-duty trucks, medium-duty passenger vehicles, heavy-duty passenger vehicles, taxis, and buses in Xi'an from 2010 to 2020 were obtained from the Shaanxi Statistical Yearbook and the Xi'an Statistical Yearbook.

2.5 WRF-CMAQ Model

2.5.1 WRF Model Setting

In this simulation, version 4.1.1 of the WRF model was utilized[13], employing meteorological field data with a horizontal resolution of 1°×1° and a temporal resolution updated every 6 hours. These data were sourced from the Final Analysis (FNL) global analysis dataset provided by the National Centers for Environmental Prediction (NCEP). A three-layer nested grid configuration was implemented to enhance the simulation accuracy in localized regions. The grid configurations were as follows: the d01 layer had a horizontal resolution of 27 km with a grid layout of 43×70; the d02 layer had a horizontal resolution of 9 km with the same grid layout of 43×70; and the d03 layer had a further refined horizontal resolution of 3 km with a grid layout of 46×73. The simulation output interval was set to every 3 hours. The parameterization schemes employed are listed in Table 3.

Table 3. Parameter settings for WRF model

Model Parameter	Parameterization Scheme
Projection Parameter	Lambert Conformal Projection
Vertical Layer	30 vertical layers, terrain-following coordinates
Meteorological Background Field	1°×1° FNL analysis data, 6-hour input interval
Longwave Radiation	RRTMG Radiation Scheme
Shortwave Radiation	Goddard Radiation Scheme
Boundary Layer	YSU Scheme

2.5.2 CMAQ Model Setting

In this study, the simulation domain for the CMAQ model was determined by cropping the innermost grid (d03) of the WRF model using the Meteorology-Chemistry Interface Processor (MCIP) module[14][15]. To optimize simulation efficiency and accuracy, the outermost three layers of grids were removed from the simulation domain. After edge cropping, the final simulation domain consisted of 43×70 grids, with each grid having a resolution of 3 km. The specific parameters of the simulation scheme and domain setup are detailed in Table 4.

Table 4. Parameter settings for CMAQ model

Model Parameter	Parameterization Scheme
Version	CMAQ 5.3.2
Projection	Lambert
Photochemical Mechanism	CB06R3
Aerosol Model	AER07
Vertical Layer	30 vertical layers, terrain-following coordinates
Meteorological Background Field	MCIP-processed WRFv4.1.1 d-layer data
Horizontal Resolution	3km

2.6 BenMAP-CE Model

The BenMAP-CE model was employed to assess the health impacts of PM2.5, involving the collection and analysis of the following key data[16]: (1) the spatial distribution of air quality changes; (2) the total population exposed to PM2.5 within the study area; (3) the baseline health incidence rates and exposure-response relationship coefficients in the study region. The impact of PM2.5 concentration changes on population health under different electrification scenarios is expressed by formula (6):

$$\Delta Y = Y_0 \times \left(1 - e^{-\beta \times \Delta X}\right) \times POP \quad (6)$$

In the formula, ΔY represents the number of reduced or avoided health issues due to the decrease in PM2.5 concentration under a specific electrification scenario; Y_0 denotes the baseline incidence rate of a specific health endpoint; β represents the exposure-response coefficient between PM2.5 and the health endpoint; ΔX indicates the change in the weighted annual average PM2.5 concentration under different electrification scenarios; and POP represents the total population in the assessment area potentially affected by PM2.5 concentration changes.

In this study, the assessment process of the health impacts of air pollution on residents focused on the baseline incidence rate of premature mortality[17]. Additionally, to determine the prevalence and hospitalization rates of health endpoints such as respiratory diseases, cardiovascular diseases, and chronic bronchitis, relevant data from Shaanxi Province in the "China Health and Family Planning Statistical Yearbook" were referenced. The baseline mortality or incidence rates of these health endpoints, as well as their exposure-response coefficients (β) with PM2.5 concentration changes, were comprehensively estimated based on a series of related literature, revealing the correlation between specific pollutant concentrations and health risks. Table 5 lists the exposure-response relationship coefficients and baseline incidence rates of these health endpoints:

Table 5. Exposure-response relationship coefficients (β) and baseline incidence rates for health endpoints.

Health Endpoint		β Value (95% Confidence Interval)	Baseline Incidence Rate
Premature Mortality	Chronic Effect Mortality	0.090%（0.000%，0.180%）	0.15992%

	Acute Effect Mortality	0.041%（0.032%，0.050%）	
Hospitalization	Respiratory	0.109%（0.000%，0.221%）	0.46301%
	Cardiovascular Cerebrovascular	0.068%（0.0423%，0.093%）	0.22192%
Morbidity	Chronic Bronchitis	0.270%（0.076%，0.464%）	0.28219%

3 Results and Discussion

3.1 Motor vehicle emission inventory

3.1.1 Base year motor vehicle emission inventory

In the base year, the total emissions of CO, NH3, NOX, PM2.5, PM10, VOC, and SO2 from motor vehicles in Xi'an City were 62,509.81 t, 1,499.30 t, 39,467.77 t, 737.15 t, 1,770.79 t, 7,923.46 t, and 136.28 t, respectively. There are significant differences in pollutant contribution rates among different vehicle types. Light-duty passenger vehicles are the primary pollution source, accounting for 42.82%, 47.55%, 3.82%, 22.05%, 23.91%, 39.43%, and 36.54% of the total emissions of CO, NH3, NOX, PM2.5, PM10, VOC, and SO2, respectively. Medium-duty passenger vehicles are the secondary pollution source, contributing 38.02%, 48.06%, 4.52%, 18.79%, 20.29%, 28.61%, and 36.18% of the total emissions of CO, NH3, NOX, PM2.5, PM10, VOC, and SO2, respectively. Heavy-duty passenger vehicles have the lowest emissions, releasing 2,275.65 t CO, 43.60 t NH3, 121.57 t NOX, 9.54 t PM2.5, 22.95 t PM10, 365.94 t VOC, and 1.89 t SO2. Light-duty trucks are the largest contributors to PM2.5 and PM10, accounting for 29.30% and 29.35% of the total emissions, respectively. Other pollutants, including CO, NH3, NOX, VOC, and SO2, contribute 7.01%, 0.89%, 49.57%, 10.14%, and 15.06% of the total emissions, respectively. Medium-duty trucks and heavy-duty trucks have similar emission types and proportions, including CO, NH3, NOX, PM2.5, PM10, VOC, and SO2, with NOX and PM10 being the highest contributors. Table 6 presents the total emissions of different types of vehicles in the base year.

Table 6. Base year motor vehicle emission inventory by vehicle type (t)

Type	CO	NH_3	NO_X	$PM_{2.5}$	PM_{10}	VOC	SO_2
LDV	26767.25	712.99	1506.21	162.58	423.42	3124.57	49.76
MDV	23770.19	720.59	1784.85	138.53	359.29	2267.30	49.29
HDV	2275.65	43.60	121.57	9.54	22.95	365.94	1.89
LDT	4384.22	13.34	19567.26	215.98	519.82	803.67	20.52
MDT	2458.24	3.53	8138.86	97.98	199.97	656.96	5.27
HDT	2853.86	5.15	8348.72	112.54	245.34	704.92	9.45
Total	62509.81	1499.30	39467.77	737.15	1770.79	7923.46	136.28

As emission standards improve, the total vehicle emissions show a gradual decline, but there are significant differences in pollutant contribution rates. Vehicles meeting the China I emission standard have the lowest total emissions at 1,918.63 t, with CO, NOX, and NH3 being the primary pollutants, accounting for 1.71%, 1.75%, and 1.83% of the total vehicle emissions, respectively. Vehicles meeting the China II emission standard have total emissions 5.48 times higher than China I, at 12,431.82 t, with significant increases in NOX and NH3 emissions, contributing 15.95% and 22.13% of the total vehicle emissions, respectively. Vehicles meeting the China III emission standard have total

emissions 3.28 times higher than China II, at 53,277.01 t, with CO and NOX emissions dominating, accounting for 42.71% and 54.75% of the total vehicle emissions, respectively. Vehicles meeting the China IV emission standard have total emissions 27.81% lower than China III, at 38,472.48 t, with reduced emissions of PM2.5 and PM10, contributing 39.71% and 42.44% of the total vehicle emissions, respectively. Vehicles meeting the China V emission standard have the lowest total emissions at 7,902.37 t, but VOC and SO2 emissions are relatively high, contributing 6.31% and 13.14% of the total vehicle emissions, respectively. Table 7 illustrates the total emissions of vehicles under different emission standards in the base year.

Table 7. Base year motor vehicle emission inventory by emission standard (t)

ES	CO	NH_3	NO_X	$PM_{2.5}$	PM_{10}	VOC	SO_2
China Ⅰ	1065.20	27.51	691.68	5.95	13.34	113.91	1.04
China Ⅱ	4433.35	331.76	6295.01	71.62	156.28	1134.40	9.40
ChinaⅢ	26728.55	323.31	21591.26	288.75	650.90	3658.02	36.22
ChinaⅣ	24778.24	748.87	9309.06	293.16	749.90	2521.52	71.73
China Ⅴ	5463.38	67.75	1579.89	77.66	200.26	495.56	17.87
Total	62509.81	1499.30	39467.77	737.15	1770.79	7923.46	136.28

3.1.2 Future year electrification scenario emission inventory

Table 8 presents the pollutant emissions under various electrification scenarios. The results indicate that the effectiveness of electrification in controlling gaseous pollutants is significantly superior to that of particulate matter. Specifically, the reduction rate of Volatile Organic Compounds (VOCs) reaches 88.86% in the high electrification scenario, with a total reduction of 3,894.32 tons compared to the baseline scenario. This is directly related to the elimination of evaporative emissions from fuel-powered vehicles and incomplete combustion products during cold starts. Notably, although the total emissions of Nitrogen Oxides (NOx) continue to decline with the advancement of electrification, their high baseline level (approximately 41,000 tons) in the baseline scenario means they remain a significant component of the pollutant inventory, highlighting the limitations of diesel vehicle exhaust after-treatment systems in real-world operation. In terms of particulate matter emissions, the reduction rates of PM2.5 and PM10 (68.11%-69.06%) are significantly lower than those of gaseous pollutants, revealing that the contribution of non-exhaust emission sources increases relatively with the electrification process. When the electrification rate exceeds 80%, mechanical sources such as brake wear (contributing 32%-41% of PM10 emissions) and tire wear (contributing 18%-25% of PM2.5 emissions) become dominant factors. This structural shift in emission sources poses new challenges to existing road dust control standards.

As the electrification rate increases from low (33.39%) to medium (55.72%) and high (84.45%), pollutant emissions exhibit a non-linear decreasing trend. Among them, Volatile Organic Compounds (VOCs) and Nitrogen Oxides (NOx) show the most sensitive reduction responses, achieving reduction efficiencies of 88.86% and 78.86%, respectively, in the high electrification scenario. This is primarily attributed to the dominant role of VOCs and NOx in traditional fuel-powered vehicle exhaust emissions. Notably, although the absolute emissions of particulate matter (PM2.5, PM10) and Sulfur Dioxide (SO2) continue to decrease with the increase in electrification levels, their reduction rates (68.11%-69.06% and 64.59%) are relatively lower, suggesting the potential influence of non-exhaust emission sources (e.g., brake wear, road dust). This differential reduction effect indicates that electrification technology has a more direct impact on controlling gaseous pollutants associated with traditional fuel combustion. Furthermore, the responses of different pollutants to electrification strategies exhibit significant heterogeneity. Carbon Monoxide (CO) and VOCs, as characteristic products of incomplete fuel combustion, show a strong linear correlation (R^2=0.97-0.99) between their reduction rates and the electrification rate, confirming the direct elimination of combustion-related pollutants through electrification. In contrast, the dynamic response of Ammonia (NH3) emissions exhibits a clear threshold effect: when the electrification rate increases from 42.78% (medium scenario) to 78.23% (high scenario), the slope of the NH3 reduction rate increases by 2.3 times, revealing the critical inhibitory effect of electrification on mobile source ammonia emissions.

Table 8. Emissions of Various Pollutants in Different Electrification Scenarios (t)

Scenario Settings	CO	NH3	NOX	PM2.5	PM10	VOC	SO2
Baseline Scenario	62509.81	1499.30	39467.77	737.15	1770.79	7923.46	136.28
Low Electrification	41637.47	1217.09	32435.10	570.86	1283.08	4777.05	108.49
Medium Electrification	27677.46	857.91	22786.14	459.54	1113.70	3383.80	85.54
High Electrification	9717.64	326.35	8341.87	228.05	564.69	882.73	48.26

3.2 Air Quality Simulation and Assessment in Electrification Scenarios

3.2.1 Assessment of Pollutant Simulation Results in Winter

Figure 2 illustrates the simulation results of CO, revealing a significant decrease in the average concentration of CO with the enhancement of electrification levels. Specifically, the CO concentration exhibits high-value areas centered around the road network, gradually diminishing outward from this center. In densely trafficked urban areas, CO pollution is relatively concentrated. Under the monsoon climate of Xi'an, lower temperatures lead to the formation of a pronounced temperature inversion in the atmospheric layer, causing emissions to accumulate primarily in the lower air layer, especially forming high-concentration pollution in the urban center. Additionally, the relatively low humidity and high visibility conditions in winter facilitate the dispersion of pollutants, resulting in relatively sparse pollutant concentrations in suburban areas. Under different electrification scenarios, the changes in CO concentration exhibit distinct trends. In the baseline scenario, the monthly average concentration of CO is 0.109 mg/m³, with a peak concentration of 0.288 mg/m³ and a minimum value of 0.072 mg/m³. In the low electrification scenario, the monthly average concentration decreases to 0.089 mg/m³, with a peak of 0.229 mg/m³ and a minimum value of 0.062 mg/m³. In the medium electrification scenario, the monthly average concentration of CO is 0.063 mg/m³, with a maximum value of 0.165 mg/m³ and a minimum value of 0.043 mg/m³. In the high electrification scenario, the CO concentration drops to 0.0110 mg/m³, with a peak of only 0.0325 mg/m³ and a minimum value of 0.0076 mg/m³. These results demonstrate the significant benefits of electric vehicles in reducing urban CO concentrations.

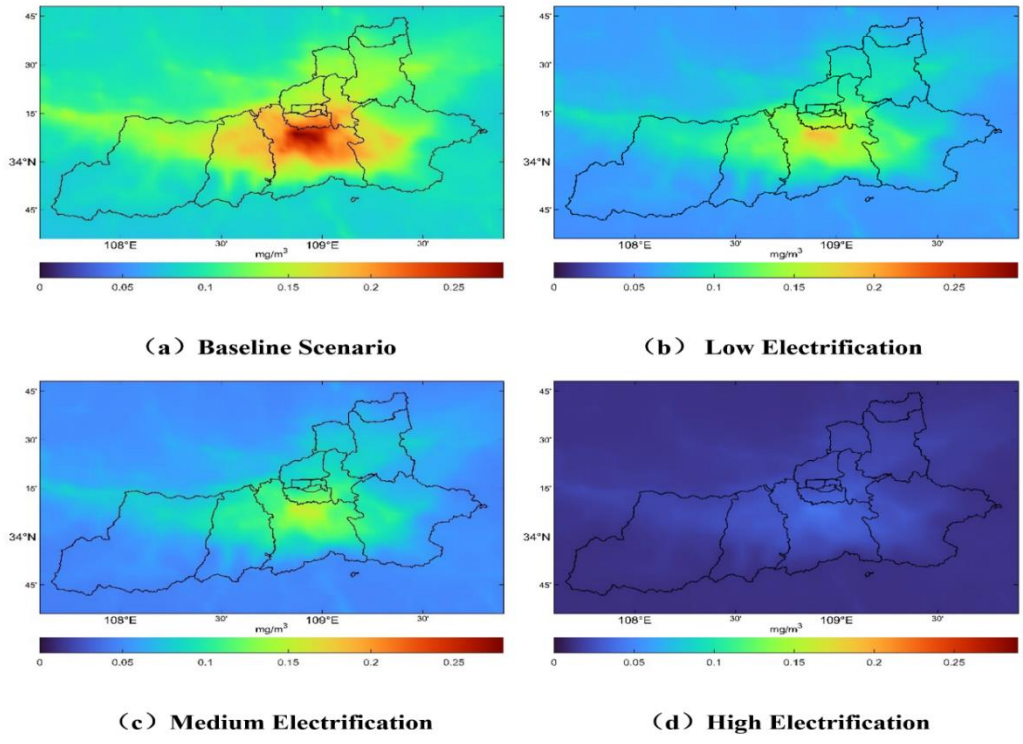

Fig.2. Spatial distribution of CO concentration under different scenarios

Figure 3 illustrates the simulation results of NO2, revealing a significant decrease in the average concentration of NO2 with the enhancement of electrification levels. The simulation results for NO_2 reveal that the concentration of NO_2 during winter is primarily distributed along the urban road network, with high-value areas concentrated. The NO_2 concentration exhibits a gradient trend that gradually decreases from the center outward, a distribution characteristic closely related to the layout of the urban road network. Under the cold winter climate, fuel-powered vehicles often require prolonged idling for warm-up during startup, which increases NO_2 emissions, particularly in urban areas with high traffic volumes. Additionally, the atmospheric stratification in winter is generally more stable, weakening vertical mixing and leading to the accumulation of pollutants in the near-surface layer. This stable atmospheric stratification, coupled with the presence of temperature inversion layers, hinders vertical air movement, further exacerbating the accumulation of NO_2 in the lower atmosphere and prolonging its residence time in the air, thereby increasing ground-level NO_2 concentrations.In the baseline scenario, the simulated monthly average NO_2 concentration is 3.665 μg/m³, with a peak concentration of 17.118 μg/m³ and a minimum concentration of 0.147 μg/m³. In the low electrification scenario, the monthly average NO_2 concentration decreases to 3.238 μg/m³, with a peak concentration of 15.113 μg/m³ and a minimum concentration of 0.124 μg/m³. In the medium electrification scenario, the monthly average NO_2 concentration further decreases to 2.522 μg/m³, with a peak value of 11.842 μg/m³ and a minimum value of 0.095 μg/m³. In the high electrification scenario, the monthly average NO_2 concentration significantly drops to 0.295 μg/m³, with a peak concentration of only 1.372 μg/m³ and a minimum concentration of 0.014 μg/m³. The simulation results demonstrate that as the level of electrification increases, NO_2 concentrations are significantly reduced, highlighting the potential role of pure electric vehicles in mitigating urban NO_2 emissions.

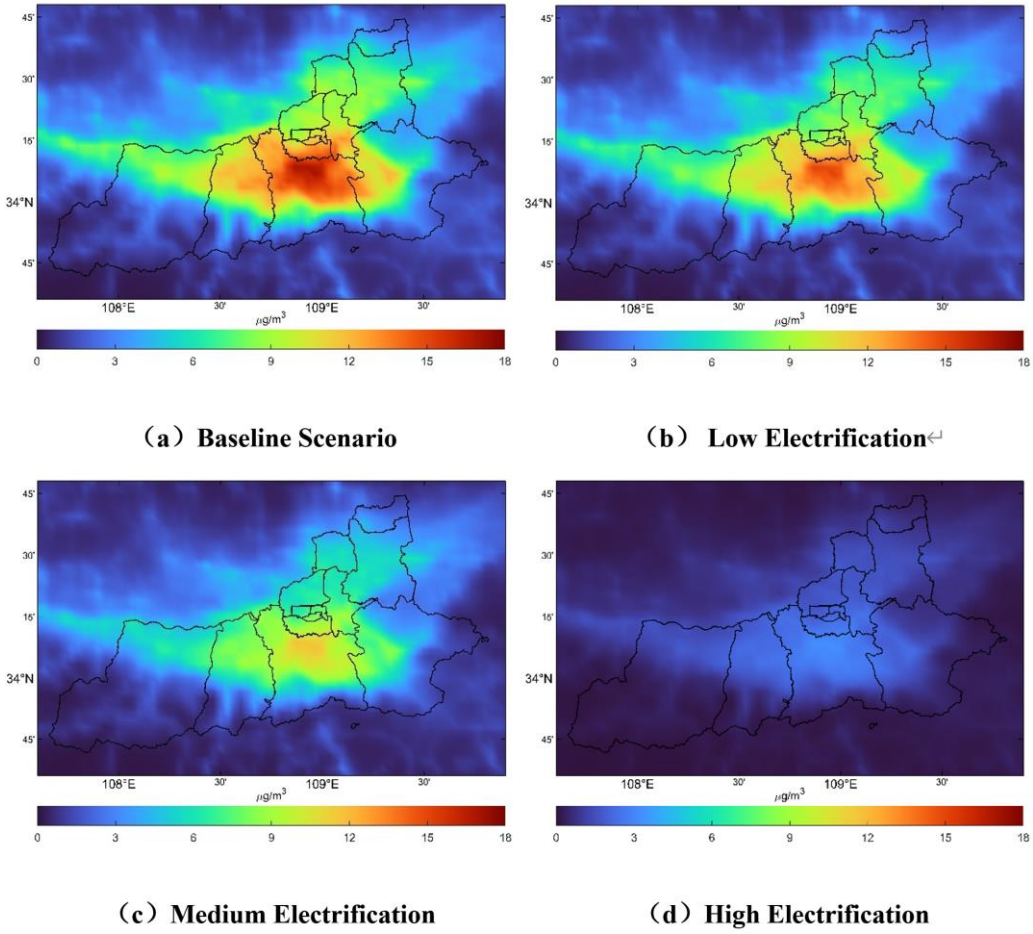

Fig.3. Spatial distribution of NO2 concentration under different scenarios

The simulation results for $PM_{2.5}$ in January reveal significant differences in $PM_{2.5}$ concentration distribution between the urban center and suburban areas. Specifically, as shown in Figure 4, the high traffic volume and complex terrain in the central urban area contribute to the accumulation of high $PM_{2.5}$ concentrations. The formation of these high-concentration areas is partly attributed to the limited dispersion and deposition of pollutants in this region. In contrast,

suburban areas exhibit relatively lower $PM_{2.5}$ concentrations, primarily due to reduced traffic volume, the purifying effect of natural vegetation, and more favorable air circulation conditions.In the baseline scenario, the simulated monthly average $PM_{2.5}$ concentration is 4.153 μg/m³, with a peak concentration of 8.319 μg/m³ and a minimum concentration of 2.295 μg/m³. In the low electrification scenario, the monthly average $PM_{2.5}$ concentration decreases to 3.176 μg/m³, with a peak concentration of 6.534 μg/m³ and a minimum concentration of 1.779 μg/m³. In the medium electrification scenario, the monthly average $PM_{2.5}$ concentration further reduces to 2.624 μg/m³, with a peak concentration of 5.317 μg/m³ and a minimum concentration of 1.449 μg/m³. In the high electrification scenario, the monthly average $PM_{2.5}$ concentration significantly drops to 1.331 μg/m³, with a peak concentration of only 2.689 μg/m³ and a minimum concentration of 0.741 μg/m³. Table 5.5 presents the $PM_{2.5}$ simulation results for different scenarios across various monitoring stations in January, clearly demonstrating the significant reduction in urban $PM_{2.5}$ concentrations with the increasing penetration of electric vehicles.

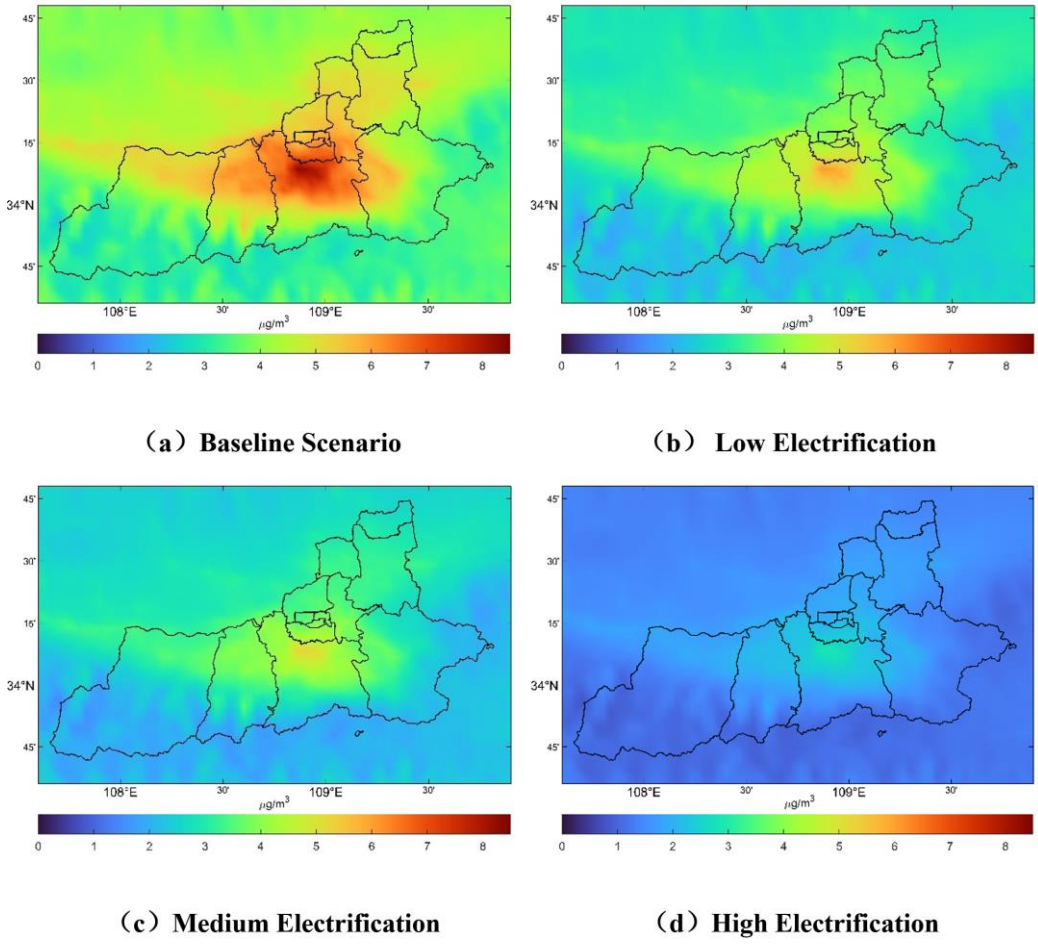

Fig.4. Spatial distribution of PM2.5 concentration under different scenarios

3.2.2 Assessment of Pollutant Simulation Results in Summer

Compared to January, CO concentrations in July generally exhibit a downward trend, particularly in the central areas of the major road network. The high concentration distribution in these regions highlights the impact of road traffic on air quality. The relatively poor atmospheric stability in summer promotes the dispersion of air pollutants, reducing the accumulation of vehicle emissions in urban centers. Additionally, intensified photochemical reactions under high-temperature conditions facilitate the oxidation of CO into substances such as carbon dioxide, further reducing CO concentrations. In the baseline scenario, the monthly average CO concentration in July is 0.0881 mg/m³, with a peak value of 0.1500 mg/m³ and a minimum value of 0.0742 mg/m³. In the low electrification scenario, the monthly average concentration decreases to 0.0722 mg/m³, with a peak concentration of 0.1226 mg/m³ and a minimum concentration of 0.0615 mg/m³. In the medium electrification scenario, the monthly average CO concentration further reduces to 0.0512 mg/m³, with a peak value of 0.0870 mg/m³ and a minimum value of 0.0457 mg/m³. In the high electrification scenario,

CO concentrations significantly decrease, with a monthly average of 0.0128 mg/m³, a peak value of 0.0336 mg/m³, and a minimum value of only 0.0089 mg/m³.

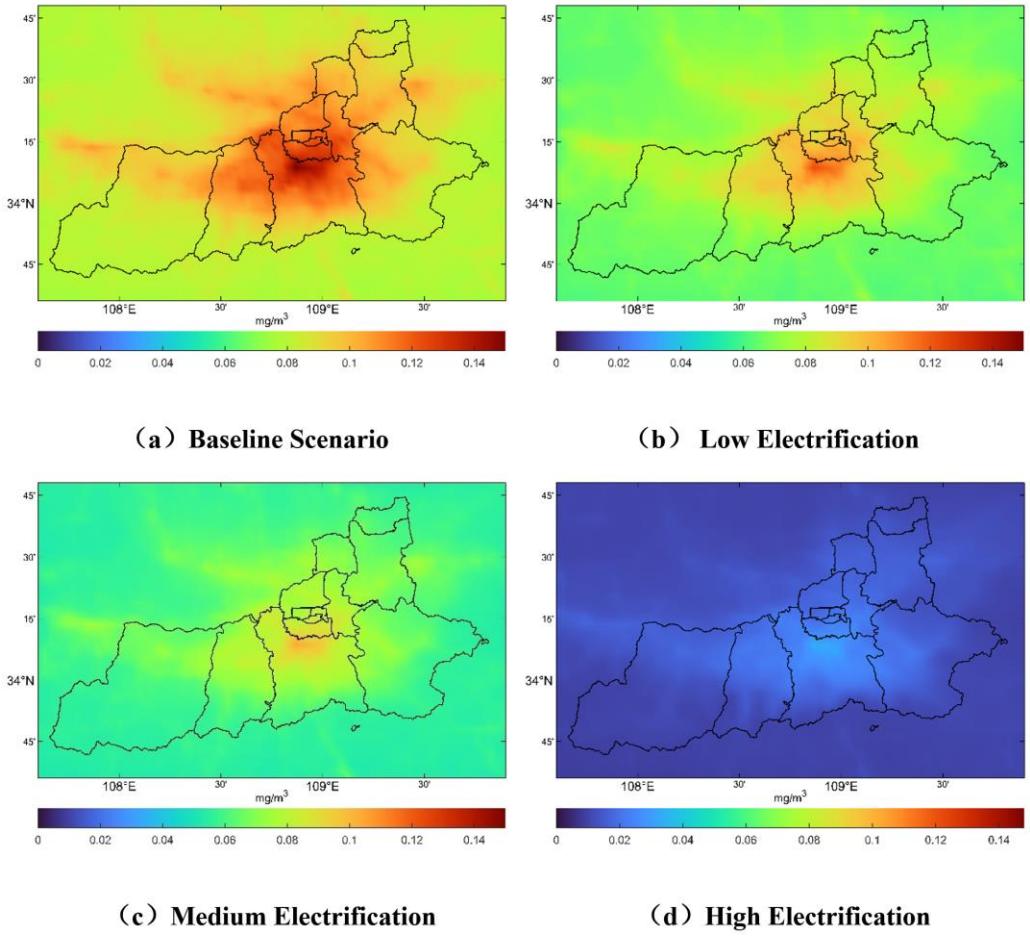

Fig.5. Spatial distribution of CO concentration under different scenarios

Compared to the data from January, the average concentration of NO_2 in July shows a significant decrease, with its distribution characteristics closely related to the urban road network. This downward trend may be influenced by multiple factors, primarily including increased summer temperatures and enhanced solar radiation. These conditions promote the photolysis of NO_2 in the atmosphere, effectively reducing its concentration. Additionally, the stability of the summer atmospheric structure, lower probability of temperature inversion layer formation, and stronger atmospheric turbulence enhance air mixing and dispersion, accelerating the dilution process of NO_2. Meteorological field data simulated by the WRF model indicate that summer wind fields and atmospheric diffusion coefficients also significantly influence the transport and distribution of NO_2. These factors collectively contribute to the dispersion of NO_2, leading to a notable reduction in NO_2 concentrations in July.Simulation results in the baseline scenario reveal that the monthly average NO_2 concentration in July is 1.368 μg/m³, with a peak concentration of 8.325 μg/m³ and a minimum concentration of 0.072 μg/m³. In the low electrification scenario, the monthly average concentration decreases to 1.209 μg/m³, with a peak concentration of 7.357 μg/m³ and a minimum concentration of 0.069 μg/m³. In the medium electrification scenario, the monthly average NO_2 concentration further reduces to 0.947 μg/m³, with a peak value of 5.761 μg/m³ and a minimum value of 0.053 μg/m³. In the high electrification scenario, the monthly average NO_2 concentration significantly drops to 0.260 μg/m³, with a peak value of only 1.581 μg/m³ and a minimum value of 0.014 μg/m³.

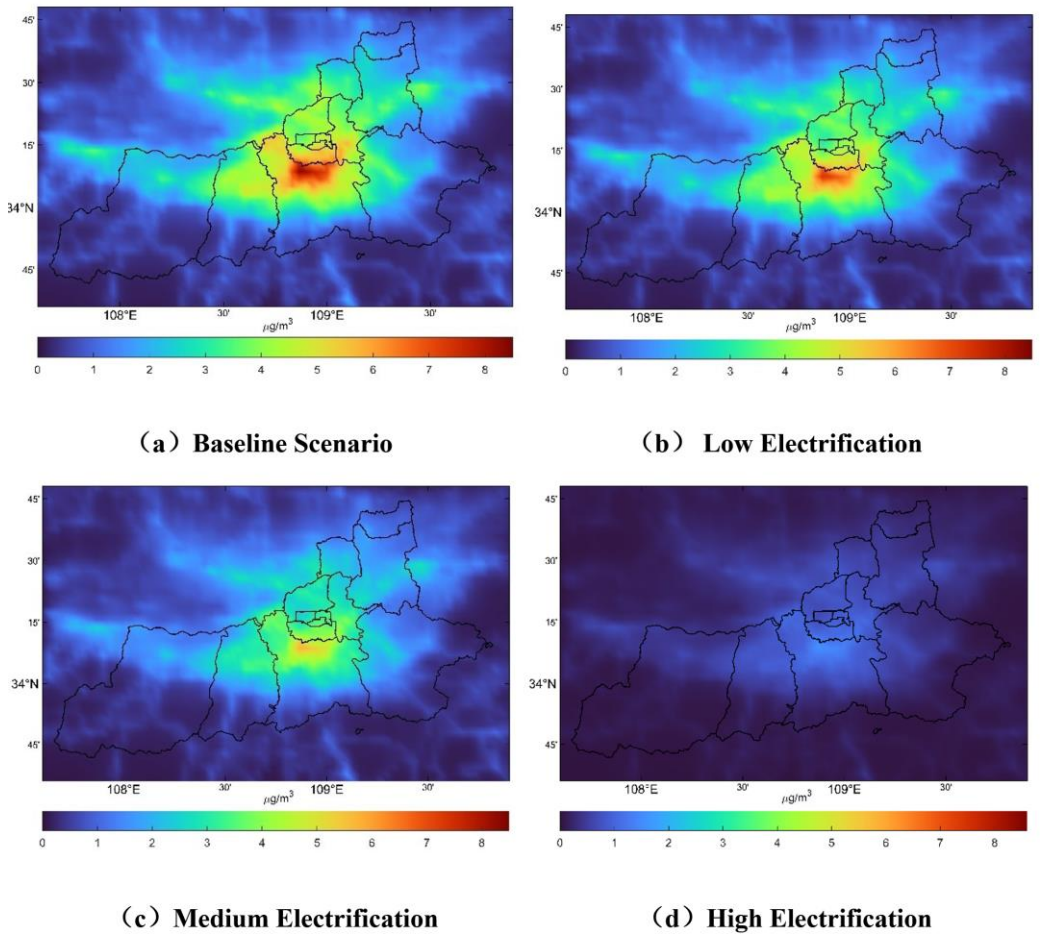

Fig.6. Spatial distribution of NO2 concentration under different scenarios

The spatial distribution characteristics of $PM_{2.5}$ in urban areas during July reveal that $PM_{2.5}$ concentrations in the city center are significantly higher than those in suburban areas, forming a gradient difference from the center to the periphery. This distribution pattern is closely related to the density of the urban road network and the higher traffic volume in the city center. Particularly at intersections and major roadways, vehicle emissions become the primary source of particulate matter. In these high-traffic-density areas, frequent vehicle idling, acceleration, and deceleration activities lead to increased $PM_{2.5}$ emissions, thereby elevating $PM_{2.5}$ concentrations in the urban center. Summer meteorological conditions, especially high temperatures and intense solar radiation, generally favor vertical atmospheric mixing, facilitating the dispersion and dilution of particulate matter in the atmosphere. Additionally, the instability of the summer atmosphere promotes vertical diffusion of pollutants, reducing their accumulation in localized areas. Simulation results show that in the baseline scenario, the monthly average $PM_{2.5}$ concentration is 3.308 μg/m³, with a peak concentration of 4.738 μg/m³ and a minimum concentration of 2.097 μg/m³. In the low electrification scenario, the monthly average concentration decreases to 2.435 μg/m³, with a peak concentration of 3.475 μg/m³ and a minimum concentration of 1.538 μg/m³. In the medium electrification scenario, the monthly average $PM_{2.5}$ concentration further reduces to 2.118 μg/m³, with a peak value of 3.015 μg/m³ and a minimum value of 1.331 μg/m³. In the high electrification scenario, the monthly average $PM_{2.5}$ concentration significantly drops to 1.0 μg/m³, with a peak value of only 0.413 μg/m³ and a minimum value of 0.186 μg/m³.

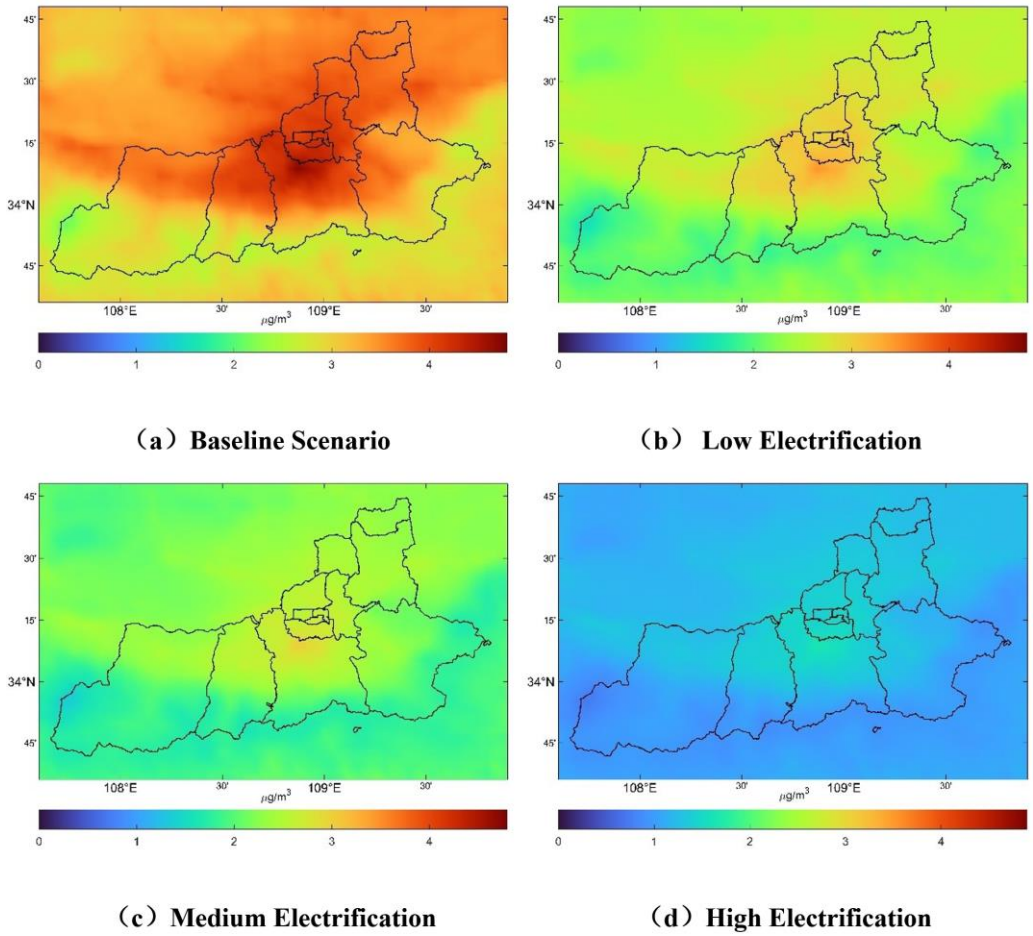

Fig.7. Spatial distribution of PM2.5 concentration under different scenarios

In summary, the spatial distribution characteristics reveal that pollutant concentrations are closely related to urban traffic volume and road network distribution. This trend is particularly evident in the main urban areas, reflecting the significant impact of traffic-intensive zones on air quality. In contrast, the simulation data for 2035 under different electrification scenarios demonstrate a notable decline in pollutant concentrations, especially in areas with heavy traffic. This indicates that the increased adoption of electric vehicles can effectively reduce vehicle emissions, thereby improving air quality in urban centers. Analysis of temporal distribution changes shows that the concentrations of CO, NO_2, and $PM_{2.5}$ in January are significantly higher than those in July. This phenomenon is associated with meteorological conditions unfavorable for pollutant dispersion in winter, such as low temperatures, reduced wind speeds, and frequent temperature inversions, as well as increased vehicle usage. However, in the electrification scenario simulations for 2035, particularly under the high electrification scenario, the difference in pollutant concentrations between winter and summer is reduced, highlighting the positive role of electric vehicles in improving air quality. The electrification scenario simulation results demonstrate that as the level of electrification increases, the concentrations of various pollutants in Xi'an generally show a downward trend. Notably, under the high electrification scenario, the reduction in pollutant concentrations in January and July is most significant, indicating the substantial potential of electric vehicles in reducing tailpipe emissions and improving urban air quality. These findings provide important scientific evidence for urban air quality management and the formulation of policies promoting electric vehicle adoption.

3.3 Health Impact Assessment of Electrification Scenarios

3.3.1 Health Endpoint Benefit Assessment

Under the electrification scenario projected for 2035, application of the BenMAP-CE model demonstrated specific health benefits related to reductions in PM2.5 concentrations. Under the low electrification scenario, an estimated 296 cases (95% CI: 65–529) of PM_2.5-related health impacts could be avoided. Enhanced health benefits were further observed under the medium electrification scenario, with an expected reduction of 474 cases (95% CI: 104–846).

Notably, the high electrification scenario yielded the most significant improvement, with up to 770 avoided cases (95% CI: 169–1375). Specifically, these health benefits primarily pertain to reductions in respiratory diseases such as chronic bronchitis. Among all health outcomes associated with PM2.5 exposure, chronic bronchitis demonstrated the greatest reduction, accounting for approximately 47% of the total health benefits. By contrast, the proportion of avoided premature deaths resulting from improved air quality was comparatively smaller, accounting for approximately 9%. These results clearly highlight the substantial benefits of promoting battery electric vehicles (BEVs) for improving air quality and mitigating PM2.5-related health issues. Therefore, widespread adoption of BEVs is anticipated to significantly reduce air pollution-induced respiratory and other health problems, consequently enhancing the overall health of urban residents.

Table 9. Health Benefits by Endpoint under Different Electrification Scenarios in 2035 (Number of Cases Avoided)

Health Endpoint		Low Electrification	Medium Electrification	High Electrification
Premature mortality	Chronic mortality	26（0，52）	42（0，83）	68（0，135）
	Acute mortality	12（9，15）	19（14，24）	31（23，39）
Hospitalization	Respiratory diseases	92（0，186）	147（0，298）	239（0，484）
	Cardiovascular Cerebrovascular	27（17，38）	43（27，61）	70（44，99）
Morbidity	Chronic bronchitis	139（39，238）	222（62，381）	361（101，619）
Total		296（65，529）	474（104，846）	770（169，1375）

Note: Values represent the estimated number of avoided cases with 95% confidence intervals provided in parentheses.

3.3.2 Health Economic Benefit Assessment

In this study, the economic impact associated with premature mortality caused by PM2.5 was assessed using the Value of Statistical Life (VSL) approach. The VSL method converts people's perceptions of health risks and their willingness-to-pay (WTP) for risk reduction into a monetary valuation of life. This approach facilitated the evaluation of the health-related economic benefits under different electrification scenarios. To reflect the economic environment in Xi'an, the VSL was adjusted to 1.7738 million CNY per individual, considering changes in per capita disposable income and GDP growth rates[18]. For estimating the economic losses associated with chronic bronchitis, a ratio equivalent to 40% of the VSL was adopted, consistent with findings from other relevant studies[19]. Furthermore, the Cost-of-Illness (COI) approach was applied to estimate economic losses for hospitalization, utilizing indicators such as average hospital stay duration and average hospitalization expenses per episode[20]. This methodology provides concrete estimates of the economic losses caused by chronic bronchitis and other health issues. By employing this comprehensive economic assessment method, quantitative insights into health-related economic benefits across different electrification scenarios were obtained. Detailed economic estimates by specific health endpoints are presented in Table 10.

Table 10. Unit Economic Costs of Various Health Endpoints in Xi'an (10^4 CNY per Case)

VSL	Hospitalization Costs		Unit Economic Cost
	Respiratory Diseases	Cardiovascular Diseases	Chronic Bronchitis
177	0.78	1.80	61.4

Based on calculations derived from the data presented in Table 11, Xi'an is expected to achieve significant economic health benefits under varying electrification scenarios by 2035. Under the low electrification scenario, the estimated economic benefits from avoided health losses amounted to 153.954 million CNY (95% CI: 40.2162–267.1114 million CNY). These benefits underscore the substantial economic returns achievable through the reduction of PM_2.5 emissions and associated health risks, even at relatively lower levels of FCVs penetration. In the medium electrification scenario, the projected economic benefits increased to 246.3264 million CNY (95% CI: 64.3459–427.3782 million CNY), indicating that a higher proportion of fuel cell electric vehicles (FCEVs) in the vehicle fleet corresponds to enhanced air quality and reduced health-related costs. The highest estimated economic benefits were identified under the high electrification scenario, amounting to 400.2804 million CNY (95% CI: 104.5621–694.4896 million CNY). This result highlights the significant potential of widespread adoption of fuel cell vehicles in substantially decreasing PM_2.5 concentrations, health risks, and associated economic losses.

Table 11. Economic Losses Avoided by Health Endpoint under Electrification Scenarios in 2035 (10^4 CNY)

Health Endpoint		Low Electrification	Medium Electrification	High Electrification
Premature Mortality	Chronic mortality	4611.88（0，9233.76）	7379.00（0，14758.00）	11991.00（0，23982.00）
	Acute mortality	2128.56（1596.42，2660.70）	3405.69（2554.27，4257.12）	5534.25（4150.69，6917.82）
Hospitalization	Respiratory diseases	71.76（0，145.08）	114.81（0，232.12）	186.57（0，377.20）
	Cardiovascular Cerebrovascular	48.60（30.60，68.40）	77.76（48.96，109.44）	126.36（79.56，177.84）
Morbidity	Chronic bronchitis	8534.60（2394.60，14613.20）	13655.36（3831.36，23381.12）	22189.96（6225.96，37994.32）
Total		15395.40（4021.62，26711.14）	24632.64（6464.59，42737.82）	40028.04（10456.21，69448.96）

In Xi'an under different electrification scenarios projected for 2035, chronic bronchitis accounted for the largest proportion (approximately 55%) of total economic benefits associated with reductions in PM_2.5-related health endpoints. This significant share is primarily attributed to reduced medical expenditures and enhanced productivity, reflecting the prominent role of vehicle electrification in mitigating long-term respiratory illnesses. Additionally, reductions in mortality rates contributed substantially to the overall economic benefits, with chronic mortality and acute mortality accounting for approximately 30% and 14%, respectively. These findings indicate that vehicle electrification can effectively improve air quality, markedly reducing mortality risks associated with air pollution, and consequently extending the average lifespan of the population. Although the economic benefits associated with cardiovascular/cerebrovascular and respiratory diseases hospitalization were relatively minor, each representing about 0.5% of total economic benefits, improvements in these areas still constitute critical components of the overall health benefits derived from vehicle electrification. These results underscore that reductions in PM_2.5 concentration resulting from vehicle electrification not only significantly enhance public health and reduce mortality risks, but also yield substantial economic gains. Notably, health improvements and economic benefits are particularly pronounced for chronic respiratory conditions, such as chronic bronchitis, closely associated with air quality.

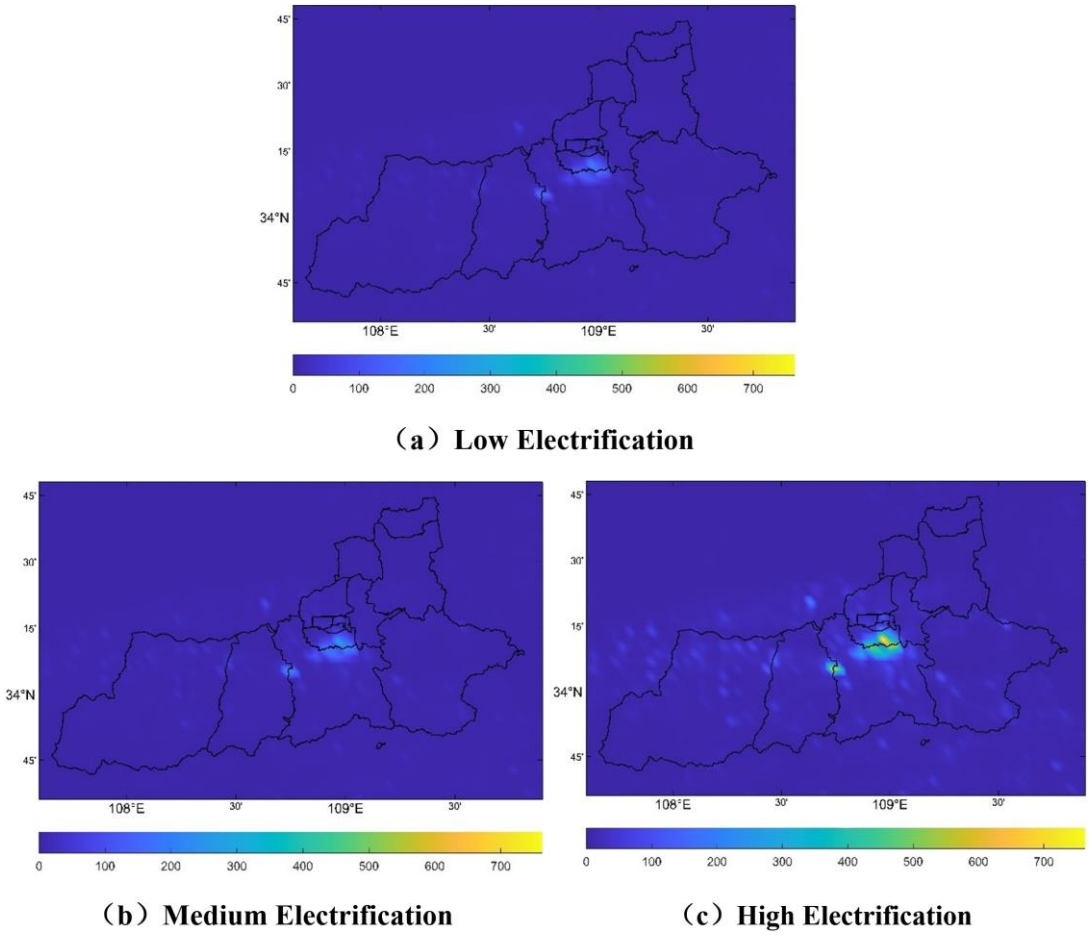

Fig.8. Spatial Distribution of Avoided Economic Losses from Premature Mortality under Different Electrification Scenarios

Figure 8 shows the spatial distribution of avoided economic losses under different electrification scenarios. It indicates notably higher reductions in economic losses within densely populated urban areas of Xi'an, primarily due to the high population density and greater sensitivity to PM2.5-related health risks. Calculations revealed that under the low electrification scenario, avoided economic losses accounted for approximately 0.0060% of Xi'an's GDP in 2035. This demonstrates that even moderate promotion of fuel cell vehicles (FCVs) can meaningfully reduce health risks and economic losses associated with air pollution. In the medium electrification scenario, this share increased to about 0.0096% of the city's GDP, highlighting that increasing FCV penetration can significantly enhance health and economic outcomes. Under the high electrification scenario, avoided economic losses reached approximately 0.0156% of Xi'an's GDP,

underscoring the substantial potential of widespread FCV adoption in mitigating health risks and economic costs from air pollution. Notably, the central urban districts exhibited considerably higher reductions compared to other areas across all scenarios, emphasizing the significant influence of population density and regional pollution levels on health risks and associated economic impacts.

4 Conclusion

In this study, the COPERT model was employed to quantify vehicle emissions under different scenarios in Xi'an. A baseline scenario and low-, medium-, and high-electrification scenarios for the year 2035 were established based on varying policy directions. Detailed analyses were conducted for January and July, representing high- and low-pollution months, respectively. The study primarily focused on assessing the impacts of different electrification scenarios on concentrations of pollutants such as CO, NO_2, and $PM_{2.5}$. Additionally, the BenMAP-CE model was used to evaluate the public health implications associated with vehicle electrification in Xi'an.

The vehicle emission inventory in Xi'an exhibited several distinct characteristics. Passenger cars were identified as the largest contributors, emitting substantial amounts of CO, NH_3, and NO_X, among which NH_3 accounted for 47.55%. Medium-sized passenger vehicles primarily emitted CO, NH_3, and SO_2, with contributions of 38.02%, 48.06%, and 36.18%, respectively. Vehicles conforming to China III and China IV emission standards represented the main sources of pollution across multiple pollutants, with China III vehicles contributing up to 54.71% of total NO_X emissions. Vehicles complying with China V and higher emission standards displayed significantly lower emissions, particularly for NO_X and particulate matter. As the level of electrification increased, emissions of all vehicle-source pollutants showed a downward trend, with reductions ranging from 17.82% to 39.71% in the low-electrification scenario, 37.11% to 57.29% in the medium-electrification scenario, and 64.59% to 98.86% in the high-electrification scenario. Correspondingly, the proportion of vehicle-source emissions relative to total atmospheric pollution decreased from the baseline to the high-electrification scenario.Simulation results obtained from the CMAQ model indicated substantial decreases in pollutant concentrations under various electrification scenarios, particularly in high-electrification scenarios and within traffic-intensive regions. Additionally, the seasonal disparity in pollutant concentrations between winter and summer was observed to diminish under the high-electrification scenario. Simulation outcomes further demonstrated that pollutant concentrations in Xi'an generally decreased as electrification levels increased, with the most notable reductions occurring in January and July under the high-electrification scenario.Health impact assessments conducted using the BenMAP-CE model for Xi'an under different electrification scenarios in 2035 indicated substantial public health benefits arising from reduced $PM_{2.5}$ concentrations, especially regarding respiratory diseases and chronic bronchitis. Significant health benefits were also observed in terms of reduced chronic and acute mortality, as well as decreased cardiovascular diseases. Economically, reductions in chronic bronchitis, chronic mortality, and acute mortality yielded the most significant contributions. Regional analysis revealed that avoided premature mortality cases and economic benefits were primarily concentrated in the central urban area, becoming more pronounced as electrification intensified. Although other districts exhibited comparatively smaller health benefits, they still presented notable potential for development.

However, several uncertainties inherent in this study could affect the accuracy and reliability of results. Due to dynamic policy and market developments, the prediction of vehicle numbers for 2035 was based solely on theoretical models. Additionally, with advancements in vehicle technology, corresponding emission factors are expected to evolve. Future studies should consider interdisciplinary predictive models and incorporate actual emission testing data from vehicles to improve the accuracy of emission inventories. The use of CMAQ and WRF models also involves numerous parameter selections, and different choices may significantly affect simulation results. Moreover, the simulation scale of the CMAQ model can influence precision. It is recommended that future research adopt broader simulation scales and more refined grids (e.g., 1 km × 1 km) to enhance the accuracy of simulation outcomes. Furthermore, the CMAQ simulation results in this study only covered January and July, limiting the comprehensive representation of annual pollutant distributions and potentially affecting BenMAP-CE model outcomes. Additionally, uncertainties regarding future population distribution and population growth may impact health assessment results. To increase assessment accuracy, future research could collaborate with other institutions to acquire more precise population distribution data.

Data Sharing Agreement

The datasets used and/or analyzed during the current study are available from the corresponding author on reasonable req uest.

Competing Interests

The authors have no relevant financial or non-financial interests to disclose.

Acknowledgment

This article was supported by Scientific Innovation Practice Project of Postgraduates of Chang'an University.

References

[1] Gan, Y., Lu, Z. F., Cai, H., Wang, M., He, X., & Przesmitzki, S. (2020). Future private car stock in China: current growth pattern and effects of car sales restriction. Mitigation and Adaptation Strategies for Global Change, 25(3), 289-306. https://doi.org/10.1007/s11027-019-09868-3

[2] Van Fan, Y., Perry, S., Klemes, J. J., & Lee, C. T. (2018). A review on air emissions assessment: Transportation [Review]. *Journal of Cleaner Production*, *194*, 673-684. https://doi.org/10.1016/j.jclepro.2018.05.151

[3] Figenbaum, E. (2017). Perspectives on Norway's supercharged electric vehiclepolicy policy. *Environmental Innovation and Societal Transitions*, *25*, 14-34. https://doi.org/10.1016/j.eist.2016.11.002

[4] Zhao, X. L., Zhao, Z. Y., Mao, Y. M., & Li, X. M. (2024). The role of air pollution in electric vehicle adoption: Evidence from China. *Transport Policy*, *154*, 26-39. https://doi.org/10.1016/j.tranpol.2024.05.022

[5] Rizza, V., Torre, M., Tratzi, P., Fazzini, P., Tomassetti, L., Cozza, V., Naso, F., Marcozzi, D., & Petracchini, F. (2021). Effects of deployment of electric vehicles on air quality in the urban area of Turin (Italy). *Journal of Environmental Management*, *297*, 9, Article 113416. https://doi.org/10.1016/j.jenvman.2021.113416

[6] Requia, W. J., Mohamed, M., Higgins, C. D., Arain, A., & Ferguson, M. (2018). How clean are electric vehicles? Evidence-based review of the effects of electric mobility on air pollutants, greenhouse gas emissions and human health [Review]. *Atmospheric Environment*, *185*, 64-77. https://doi.org/10.1016/j.atmosenv.2018.04.040

[7] Liu, F. Q., Zhao, F. Q., Liu, Z. W., & Hao, H. (2018). The impact of fuel cell vehicle deployment on road transport greenhouse gas emissions: The China case. International Journal of Hydrogen Energy, 43(50), 22604-22621. https://doi.org/10.1016/j.ijhydene.2018.10.088

[8] Mac Kinnon, M., Shaffer, B., Carreras-Sospedra, M., Dabdub, D., Samuelsen, G. S., & Brouwer, J. (2016). Air quality impacts of fuel cell electric hydrogen vehicles with high levels of renewable power generation. International Journal of Hydrogen Energy, 41(38), 16592-16603. https://doi.org/10.1016/j.ijhydene.2016.07.054

[9] Yan, J. J., Jing, J., & Li, Y. F. (2024). Hydrogen fuel cell commercial vehicles in China: Evaluation of carbon emission reduction and its economic value. International Journal of Hydrogen Energy, 52, 734-749. https://doi.org/10.1016/j.ijhydene.2023.04.164

[10] Li, Y., Miao, L., Chen, Y., & Hu, Y. K. (2019). Exploration of Sustainable Urban Transportation Development in China through the Forecast of Private Vehicle Ownership. *Sustainability*, *11*(16), 18, Article 4259. https://doi.org/10.3390/su11164259

[11] Li, Y., Huang, S. Y., Liu, Y. H., & Ju, Y. Y. (2021). Recycling Potential of Plastic Resources from End-of-Life Passenger Vehicles in China. *International Journal of Environmental Research and Public Health*, *18*(19), 15, Article 10285. https://doi.org/10.3390/ijerph181910285

[12] Liu, Y. H., Liao, W. Y., Lin, X. F., Li, L., & Zeng, X. L. (2017). Assessment of Co-benefits of vehicle emission reduction measures for 2015-2020 in the Pearl River Delta region, China. *Environmental Pollution*, *223*, 62-72. https://doi.org/10.1016/j.envpol.2016.12.031

[13] Thongthammachart, T., Araki, S., Shimadera, H., Eto, S., Matsuo, T., & Kondo, A. (2021). An integrated model combining random forests and WRF/CMAQ model for high accuracy spatiotemporal PM_{2.5} predictions in the Kansai region of Japan. *Atmospheric Environment*, *262*, 10, Article 118620. https://doi.org/10.1016/j.atmosenv.2021.118620

[14] Li, Y., Carlton, A. G., & Shiraiwa, M. (2021). Diurnal and Seasonal Variations in the Phase State of Secondary Organic Aerosol Material over the Contiguous US Simulated in CMAQ. *Acs Earth and Space Chemistry*, *5*(8), 1971-1982. https://doi.org/10.1021/acsearthspacechem.1c00094

[15] Qi, Q., Wang, S., Zhao, H., Kota, S. H., & Zhang, H. L. (2023). Rice yield losses due to O3 pollution in China from 2013 to 2020 based on the WRF-CMAQ model. *Journal of Cleaner Production*, *401*, 12, Article 136801. https://doi.org/10.1016/j.jclepro.2023.136801

[16] Sacks, J. D., Lloyd, J. M., Zhu, Y., Anderton, J., Jang, C. J., Hubbell, B., & Fann, N. (2018). The Environmental Benefits Mapping and Analysis Program - Community Edition (BenMAP-CE): A tool to estimate the health and economic benefits of reducing air pollution. *Environmental Modelling & Software*, *104*, 118-129. https://doi.org/10.1016/j.envsoft.2018.02.009

[17] Davidson, K., Hallberg, A., McCubbin, D., & Hubbell, B. (2007). Analysis of PM2.5using the Environmental Benefits Mapping and Analysis Program (BenMAP) [; Proceedings Paper]. Journal of Toxicology and Environmental Health-Part a-Current Issues, 70(3-4), 332-346. https://doi.org/10.1080/15287390600884982

[18] Yu, M., Ma, Q., Zhu, M., Zhang, J., Wang, K., Xu, Q., & Zhang, R. (2021). Evaluation for impact on PM2.5 pollution and healthy benefits of rural scattered coal replacement-a case study of Henan Province. *China Environmental Science*, *41*(8), 3906-3916, Article 1000-6923(2021)41:8<3906:Ncsmtd>2.0.Tx;2-1. <Go to ISI>://CSCD:7028451

[19] Fu, X. S., Li, L., Lei, Y. L., Wu, S. M., Yan, D., Luo, X. M., & Luo, H. (2020). The economic loss of health effect damages from PM2.5 pollution in the Central Plains Urban Agglomeration. *Environmental Science and Pollution Research*, *27*(20), 25434-25449. https://doi.org/10.1007/s11356-020-08560-3

[20] Mu, Q., & Zhang, S.-q. (2013). An evaluation of the economic loss due to the heavy haze during January 2013 in China. *China Environmental Science*, *33*(11), 2087-2094. <Go to ISI>://INSPEC:14423718